Available online at www.sciencedirect.com
ScienceDirect
Annals of Physics 322 (2007) 677–700
ANNALS of PHYSICS
www.elsevier.com/locate/aop

Superluminal cascade spectra of TeV γ-ray sources

Roman Tomaschitz *

Department of Physics, Hiroshima University, 1-3-1 Kagami-yama, Higashi-Hiroshima 739-8526, Japan

Received 2 March 2006; accepted 10 November 2006
Available online 4 January 2007

Abstract

Astrophysical radiation sources are scrutinized in search of superluminal γ-rays. The tachyonic spectral densities generated by ultra-relativistic electrons in uniform motion are fitted to the high-energy spectra of Galactic supernova remnants, such as RX J0852.0−4622 and the pulsar wind nebulae in G0.9+0.1 and MSH 15-52. The superluminal spectral maps of the unidentified TeV γ-ray sources HESS J1303−631, TeV J2032+4130 and HESS J1825−137 are inferred from EGRET, HEGRA and HESS data. Tachyonic cascade spectra are quite capable of generating the spectral curvature seen in double-logarithmic plots, as well as the extended spectral plateaus defined by EGRET flux points in the GeV band. The curvature of the TeV spectra is intrinsic, caused by the Boltzmann factor in the source densities. The spectral averaging with thermal and exponentially cut power-law electron densities can be done in closed form, and systematic high- and low-temperature expansions of the superluminal spectral densities are derived. Estimates on the electron/proton populations generating the tachyon flux are obtained from the spectral fits, such as power-law indices, temperature and source counts. The cutoff temperatures of the source densities suggest ultra-high-energy protons in MSH 15-52, HESS J1825−137 and TeV J2032+4130.

PACS: 03.50.Kk; 05.30.Ch; 11.10.Lm; 95.30.Gv

Keywords: Superluminal radiation; Tachyonic γ-rays; Cosmic rays; Spectral averaging; Spectral curvature

* Fax: +81 824 240717.
E-mail address: tom@geminga.org

0003-4916/$ - see front matter
doi:10.1016/j.aop.2006.11.005

1. Introduction

The traditional way to introduce faster-than-light particles (tachyons) is to start with the Lagrangian

$$L = -m_{\mathrm{t}}\sqrt{\eta_{\alpha\beta}\dot{x}^\alpha\dot{x}^\beta} + eA_\alpha\dot{x}^\alpha, \tag{1.1}$$

$\eta_{\alpha\beta} = \mathrm{diag}(-1,1,1,1)$, $m_{\mathrm{t}} > 0$, which differs from the Lagrangian of a classical subluminal particle just by a minus sign under the root [1–4]. The superluminal particle is coupled by minimal substitution to the electromagnetic field as indicated, if it carries electric charge e. In this article, a very different approach to superluminal signals is investigated, a Proca equation with negative mass-square, very contrary to the prevailing view of tachyons as electrically charged point particles (1.1). The Proca field is coupled to a current of subluminal massive particles, the Lagrangians of the superluminal radiation field and a subluminal classical particle coupled to this field read

$$L_{\mathrm{Proca}} = -\tfrac{1}{4}F_{\alpha\beta}F^{\alpha\beta} + \tfrac{1}{2}m_{\mathrm{t}}^2A_\alpha A^\alpha + A_\alpha j^\alpha, \tag{1.2}$$

$$L = -m\sqrt{-\eta_{\alpha\beta}\dot{x}^\alpha\dot{x}^\beta} + qA_\alpha\dot{x}^\alpha, \tag{1.3}$$

respectively, where m_{t} is the mass of the Proca field A_α. The mass term in (1.3) is added with a positive sign, so that $m_{\mathrm{t}}^2 > 0$ is the negative mass-square of the tachyonic radiation field. The subluminal particle of mass m as defined by (1.3) is supposed to carry tachyonic charge q, analogous to but independent of electric charge, by which it couples to the tachyon potential via a current $j^0 = \rho = q\delta(\mathbf{x}-\mathbf{x}(t))$, $\mathbf{j} = q\mathbf{v}\delta(\mathbf{x}-\mathbf{x}(t))$. Evidently, the Proca Lagrangian is designed in analogy to electrodynamics, but is otherwise unrelated to electromagnetic fields, and the real vector potential A_α is itself a measurable quantity, as the mass term breaks the gauge invariance. Tachyons emerge as an extension of the photon concept, a sort of photons with negative mass-square [5,6]. The superluminal radiation field does not carry any kind of charge, tachyonic charge q is a property of subluminal particles, as is electric charge. In the geometrical optics limit of this field theory, one can still describe superluminal rays by the Lagrangian (1.1) with the interaction term dropped, but otherwise the new concept is subluminal source particles emitting superluminal radiation. The negative mass-square thus refers to the radiation rather than the source, in strong contrast to the traditional approach based on superluminal source particles emitting electromagnetic radiation [1,4].

At first sight, the formalism closely resembles electrodynamics, but there are differences as well. Apart from the superluminal speed of the quanta, the radiation is partially longitudinally polarized [7]. A basic feature of photons traveling over cosmological distances is their ability to propagate dispersion free, as the wave fields are conformally coupled to the background metric. This property is also retained for tachyons, as the tachyon mass scales inversely with the cosmic expansion factor [5]. There is no interaction of tachyons with photons, they couple only indirectly via matter fields. Therefore, contrary to electromagnetic γ-rays, high-energy tachyons cannot interact with the infrared background radiation, so that there is no attenuation of the extragalactic tachyon flux due to electron–positron pair creation.

The most pronounced difference between electromagnetic and tachyonic radiation lies in the emission process itself. Freely moving electrons can radiate superluminal quanta.

Radiation densities attached to a uniformly moving charge have no analog in electrodynamics, their very existence has substantial implications for the space–time structure, requiring an absorber that breaks the time symmetry of the emission process [8]. The tachyonic radiation densities depend on the velocity of the uniformly moving charge in the rest frame of the cosmic absorber, and there is a radiation threshold, a minimal speed for superluminal radiation to occur [9]. The Green function of this radiation process is time-symmetric, there is no retarded propagator supported outside the lightcone. The advanced modes of the radiation field are converted into retarded ones by virtue of a non-local, instantaneous interaction with the cosmic absorber medium [10]. The latter also defines a universal frame of reference necessary to render the superluminal signal transfer causal. The time symmetry of the Green function implies that there is no radiation damping, the radiating charge stays in uniform motion. The energy radiated is supplied by the oscillators constituting the absorber medium.

The quantization of superluminal field theories has constantly been marred by the fact that there is no relativistically invariant way to distinct positive and negative frequency solutions outside the lightcone, a consequence of time inversions by Lorentz boosts. When attempting quantization, the result was either unitarity violation or a non-invariant vacuum state [2,4]. Therefore, relativistic interactions of superluminal quanta with matter have never been worked out to an extend that they could be subjected to test. In fact, tachyons have not been detected so far, and one may ask why. There is the possibility that superluminal signals just do not exist, the vacuum speed of light being the definitive upper bound. In an open universe, however, this is not a particularly appealing perspective. There is another explanation, the interaction of superluminal radiation with matter is very weak, the quotient of tachyonic and electric fine structure constants being $\alpha_q/\alpha_e \approx 1.4\times 10^{-11}$, and therefore superluminal quanta are just hard to detect [5]. There have been searches for superluminal particles, which were assumed to be electrically charged sources of vacuum Cherenkov radiation, and bubble-chamber events were reanalyzed in search of negative mass-squares inferred from energy–momentum conservation [11]. Apart from that, tachyonic quanta should have been detected over the years, accidentally, despite of their tiny interaction with matter. The most likely reason as to why this has not happened is this: Due to our contemporary spacetime conception, we are obliged to systematically ignore them.

In fact, in a relativistic spacetime view, superluminal signals are causality violating, irrespectively of the special mechanism of the transmission. If two events are connected by a tachyonic signal, a Lorentz boost can interchange the time order, so that some observers will see the effect preceding the cause, absorption preceding emission, for instance [4]. Hence, outside the lightcone, in the domain of tachyonic signal transfer, there is no relativistically invariant meaning to cause and effect. Clearly, there are acausal solutions in electrodynamics as well, advanced wave fields, and even in Newtonian mechanics one can easily specify acausal initial conditions such as a negative time delay. However, these solutions can be identified and discarded on the grounds of causality violation. When superluminal signals are involved in a relativistic context, this cannot be done, as there is no invariant way to distinct causal from acausal solutions. What appears causal to one observer is acausal to others, since Lorentz boosts can invert the time order of spacelike connections. This is in strong contrast to the retarded wave fields of electrodynamics, which stay retarded in all frames. Retarded superluminal waves, however, will usually acquire an advanced acausal component if subjected to Lorentz boosts. Superluminal

signals are thus incompatible with the relativity principle, as they unavoidably entail causality violation, quite independently of the physical mechanism of the signal transfer [5]. This suggests to use an absolute spacetime conception when dealing with tachyons. Relativity theory is a theory of subluminal motion, and the extension of the relativity principle to spacelike connections conflicts with causality. To reconcile superluminal signals with the causality principle, it is necessary to find an absolute time order as defined by cosmic time in the comoving galaxy frame, the rest frame of the absorber medium. The cosmic time order unambiguously determines the causality of events connected by superluminal signals. All observers can arrive at the same conclusion by synchronizing their proper time with cosmic time, irrespectively of time inversions that may occur in individual rest frames [10]. Had there been detection in the above mentioned searches, in the relativistic framework in which they were interpreted, this would have been tantamount to causality violation. By contrast, the radiation mechanism suggested here, based on a Proca field with negative mass-square minimally coupled to subluminal matter, is non-relativistic, as it invokes the absolute spacetime defined by the absorber, even though the Lagrangians are covariant.

Unitarity violation [12], an unstable vacuum [4] and causality violation [13] are inextricably linked with relativistic superluminal field theories. Unitarity violation means that the quantum mechanical probability amplitude is not conserved, an incurable inconsistency. The term 'unstable vacuum' is a misnomer suggesting that there are field theories with a stable vacuum and others with an unstable one, just like stable and unstable dynamical systems. An unstable vacuum, however, has nothing to do with dynamical instability. It is an inconsistency arising in quantization attempts of relativistic superluminal theories and implies an energy functional unbounded from below, so that one ends up with a finite system from which an infinite amount of energy can be extracted, a perpetuum mobile. Indefinite energy functionals can be traced back to causality violation endemic in relativistic theories of superluminal signal transfer. Attempts to cure the problem of negative energies in terms of an antiparticle reinterpretation analogous to the Dirac Hamiltonian have failed, as causality remains violated [4]; the indefinite classical energy functional of the Dirac theory is not related to causality violation, after all.

The technical reason why it is not possible to consistently define a positive definite energy functional in a relativistic superluminal field theory is elementary and does not depend on the specific modeling of the signal transfer. Lorentz boosts can change the sign of the energy component of a spacelike 4-momentum, so that negative frequency modes are generated, which can be made arbitrarily large by choosing a suitable boost. This is also the root of causality violation; Lorentz boosts can change the time order of spacelike connections, so that one can always find inertial frames in which the effect precedes the cause.

It has been argued that causality-violating signal transfer outside the lightcone is not a logical inconsistency [13], implying that the only way to figure out whether tachyons comply with the causality principle is to find them and to settle this empirically. This is presumably true, but the trouble here is that relativistic acausal theories have been very inefficient with regard to suggestions where to look for tachyons. Causality may not be a logical necessity, but it is a practical one regarding physical modeling. Without supposition of the causality principle (that is, every effect has a cause, the cause precedes the effect, and the terms cause and effect can be invariantly attached to the respective events) one will most likely spend one's time solving causality paradoxa [14] rather than calculating cross sections, the latter being indispensable for quantitative suggestions as to where to find tachyons.

A consistent quantization, implying causality, a stable vacuum and a unitary scattering matrix, can be achieved if we refrain from modeling superluminal signals on the basis of a local relativistic spacetime and invoke an absolute time order instead when dealing with spacelike momenta. The criterion for the usefulness of any given spacetime conception, the use of an expanding 3-space in cosmology to model redshifts for instance, is efficiency regarding physical modeling in a given context. A spacetime concept has no physical reality by itself and has to be adapted to the context, not the other way round. We employ an absolute spacetime for the modeling of superluminal signal transfer, since an extension of the relativistic spacetime concept to spacelike momenta is counterproductive in dealing with superluminal signals.

A relativistic spacetime conception has at its core the Galilean assertion of the equivalence of uniform motion and rest. The laws of physics are the same in all inertial frames, the latter are considered equivalent and synchronized by a group of coordinate transformations such as Lorentz boosts. In particular, there is no distinguished state of rest, the substitute for this is uniform inertial motion. One can even single out a preferred frame, such as the comoving galaxy frame defining cosmic time, this is still a relativistic concept.

An absolute space is defined by a microscopic space structure replacing the purely geometric Euclidean space concept of coordinate axes labeling the void. We assume that this space structure is a Wheeler–Feynman absorber medium [8] capable of turning advanced superluminal wave modes into retarded ones. The absorber defines the frame of absolute rest coinciding with the comoving galaxy frame, so that cosmic time provides the universal time order required in the causality principle. The absolute spacetime concept is centered at the state of rest, accelerated and inertial frames are based on this reference frame. The superluminal spectral densities studied in Section 2 are determined by the velocity of the radiating charge. This is not a relative velocity, it stands for the absolute motion of the charge in the absorber medium.

The absorber medium reminds us of the prerelativistic ether outlawed by relativity theory [15]; Michelson–Morley cannot be invoked if the absorber medium does not affect electromagnetic wave propagation. When contemplating a microscopic space structure, one has to keep in mind that it has to compete with Euclidean space, already a cubic lattice structure makes physical modeling much harder. The question thus arises how to define this space structure without compromising the efficiency of Euclidean modeling. The way to proceed is suggested by the Mach principle and the Wheeler–Feynman absorber theory.

The Mach principle tries to explain the inertial force in Newton's equations by a nonlocal interaction with the mass content of the universe. In practice, it is not really necessary to know the details of this interaction, as the inertial force defines itself locally by mass and acceleration. The Wheeler–Feynman absorber theory was designed in the context of a time symmetric formulation of electrodynamics [8]. In this theory, the absorber comprises the collection of electric charges in the universe, its interaction with time symmetric electromagnetic fields is instantaneous and nonlocal and turns advanced wave modes into retarded ones. Here again, it is not necessary to quantify the details of this interaction such as the actual charge distribution, as the time symmetric Green function and the retarded and advanced wave fields generated are determined by the local Hamiltonian. A similar absorber concept is used for tachyonic wave propagation. Outside the lightcone, there are no retarded or advanced Green functions, the time symmetry of the wave propagation is broken by the absorber medium. One can give an explicit model of the absorber

medium, in terms of uniformly distributed microscopic oscillators interacting with the time symmetric wave field [16], but this is not really necessary, as the time symmetric Green function can be calculated from the local Hamiltonian [10].

It is the interaction mechanism with matter rather than the space and causality conception that provides the clues where to search for tachyons. We work out specific examples, scrutinizing astrophysical radiation sources for superluminal γ-rays. We perform tachyonic spectral fits to the spectra of Galactic supernova remnants and other recently discovered TeV γ-ray sources. In Section 2, we explain the transversal and longitudinal spectral densities generated by uniformly moving charges as well as the spectral averaging with thermal and power-law electron distributions. These spectral densities have no analog in electrodynamics; tachyonic synchrotron densities reduce to these densities in the limit of infinite bending radius [17], but electromagnetic synchrotron radiation vanishes in this limit. In Section 3, we derive the high- and low-temperature expansions of the averaged radiation densities. Tachyonic spectral maps of the supernova remnants G0.9+0.1, RX J0852.0−4622 and MSH 15-52 as well as the unidentified TeV γ-ray sources HESS J1303−631, TeV J2032+4130 and HESS J1825−137 are obtained by fitting EGRET, HEGRA and HESS flux points. We discuss spectral peaks, breaks, slopes, and the curvature of tachyonic cascade spectra. In Section 4, we compare the cutoff temperature of the electronic/protonic source populations to the break energies in the cosmic-ray spectrum, and point out the possibility of ultra-high-energy protons in at least three of the studied TeV sources. In Appendix A, we calculate the normalization factors of the spectral densities; the singular high-temperature expansions at integer electronic power-law index are dealt with in Appendix B.

2. Tachyonic spectral densities of freely moving electrons

The quantized transversal and longitudinal radiation densities of a uniformly moving spinning charge read [9]

$$p^{\mathrm{T,L}}(\omega,\gamma)=\frac{\alpha_{\mathrm{q}}m_{\mathrm{t}}^2\omega}{\omega^2+m_{\mathrm{t}}^2}\left[\gamma^2-\frac{m_{\mathrm{t}}}{m}\frac{\omega}{m_{\mathrm{t}}}\gamma-\frac{1}{4}\frac{m_{\mathrm{t}}^2}{m^2}-\left(1+\frac{\omega^2}{m_{\mathrm{t}}^2}\right)\Delta^{\mathrm{T,L}}\right]\frac{1}{\gamma\sqrt{\gamma^2-1}}, \tag{2.1}$$

where

$$\Delta^{\mathrm{T}}=1-\frac{1}{2}\frac{m_{\mathrm{t}}^2}{m^2},\quad \Delta^{\mathrm{L}}=0. \tag{2.2}$$

Here, γ is the electronic Lorentz factor, m_{t}/m the tachyon-electron mass ratio, and α_{q} the tachyonic fine structure constant. A spectral cutoff occurs at

$$\omega_{\max}(\gamma)=m_{\mathrm{t}}\left(\mu\sqrt{\gamma^2-1}-\frac{1}{2}\frac{m_{\mathrm{t}}}{m}\gamma\right),\quad \mu:=\sqrt{1+\frac{m_{\mathrm{t}}^2}{4m^2}}. \tag{2.3}$$

Only frequencies in the range $0<\omega<\omega_{\max}(\gamma)$ can be radiated by a uniformly moving charge, the tachyonic spectral densities $p^{\mathrm{T,L}}(\omega)$ are cut off at the break frequency $\omega_{\max}$. The radiation condition on the electronic Lorentz factor is $\gamma>\mu$, cf. (2.3); since $\omega_{\max}(\mu)=0$, there is no emission by uniformly moving charges with Lorentz factors $\gamma\leqslant\mu$. The threshold on the speed of the charge for radiation to occur is thus $\upsilon>\upsilon_{\min}:=m_{\mathrm{t}}/(2m\mu)$. The units $\hbar=c=1$ can easily be restored. We use the Heaviside–Lorentz

system, so that $\alpha_q = q^2/(4\pi\hbar c) \approx 1.0\times 10^{-13}$ is the tachyonic fine structure constant. The tachyon mass is $m_t \approx 2.15\ \mathrm{keV}/c^2$. These estimates are obtained from hydrogenic Lamb shifts [5]. The tachyon–electron mass ratio, $m_t/m \approx 1/238$, gives $\upsilon_{\min}/c \approx 2.1\times 10^{-3}$.

The spectral densities (2.1) are generated by a Dirac current. The spectral densities of a classical point charge are recovered by putting all m_t/m-ratios in ((2.1)–(2.3)) equal to zero, in particular, $\Delta^{\mathrm{T}}_{\mathrm{cl}} = 1$ and $\Delta^{\mathrm{L}}_{\mathrm{cl}} = 0$, and the classical spectral cutoff occurs at $\omega_{\max,\mathrm{cl}} := m_t\sqrt{\gamma^2-1}$. In the ultra-relativistic limit, $\gamma \gg 1$, we can likewise drop all terms containing m_t/m-ratios, so that the ultra-relativistic quantum densities coalesce with the classical densities. Substantial quantum effects regarding the shape of the spectral density emerge only in the extreme non-relativistic limit [9]. We may then parametrize $\gamma = \mu + \varepsilon$, with $\varepsilon \ll 1$, so that the source velocity in the vicinity of $\upsilon_{\min}$ reads

$$\upsilon = \frac{\sqrt{m_t^2/(4m^2) + 2\mu\varepsilon + \varepsilon^2}}{\mu+\varepsilon}, \tag{2.4}$$

and we may substitute $\sqrt{\gamma^2-1} = \upsilon\gamma$ in (2.1) and (2.3). If the polarization is not observed, we use the total spectral density $p^{\mathrm{T+L}}(\omega) := p^{\mathrm{T}}(\omega) + p^{\mathrm{L}}(\omega)$.

The radiation densities (2.1) refer to single charges with Lorentz factor γ. We average them with electron distributions, power-laws exponentially cut with Boltzmann distributions, $\mathrm{d}\rho \propto E^{-2-\alpha}\mathrm{e}^{-E/(kT)}\mathrm{d}^3p$, or

$$\mathrm{d}\rho_{\alpha,\beta}(\gamma) := \gamma^{-\alpha-1}\mathrm{e}^{-\beta\gamma}\sqrt{\gamma^2-1}\,\mathrm{d}\gamma, \tag{2.5}$$

where $\beta := mc^2/(kT)$. The electronic Lorentz factors range in an interval $\gamma_1 \leqslant \gamma < \infty$, the lower edge satisfies the radiation condition $\gamma_1 \geqslant \mu$, cf. after (2.3). Linear combinations of (2.5) may be used for wideband spectra, including pure power-laws, cf. the modeling of γ-ray burst spectra [18,19] and electron distributions in galaxy clusters [20]. The normalization factors $A_{\alpha,\beta}(\gamma_1,n_1)$ of densities (2.5) are determined by $n_1 = A_{\alpha,\beta}(\gamma_1,n_1)\int_{\gamma_1}^{\infty}\mathrm{d}\rho_{\alpha,\beta}(\gamma)$, where n_1 is the electron count and γ_1 the smallest Lorentz factor in the source population.

The averaging is carried out via

$$\langle p^{\mathrm{T,L}}(\omega;\gamma_1,n_1)\rangle_{\alpha,\beta} := A_{\alpha,\beta}(\gamma_1,n_1)\int_{\gamma_1}^{\infty} p^{\mathrm{T,L}}(\omega,\gamma)\theta(\omega_{\max}(\gamma)-\omega)\,\mathrm{d}\rho_{\alpha,\beta}(\gamma), \tag{2.6}$$

with $\omega_{\max}(\gamma)$ in (2.3). These averages can be reduced to the spectral functions

$$B^{\mathrm{T,L}}(\omega;\gamma;\alpha,\beta) := \int_{\gamma}^{\infty} p^{\mathrm{T,L}}(\omega,\tilde\gamma)\mathrm{d}\rho_{\alpha,\beta}(\tilde\gamma), \tag{2.7}$$

where $\gamma \geqslant \mu$. More explicitly,

$$B^{\mathrm{T,L}}(\omega;\gamma;\alpha,\beta) = \frac{\alpha_q m_t\hat\omega}{1+\hat\omega^2}\frac{1}{\gamma^{\alpha+1}\beta^2}\left\{\left[(1+\alpha)\alpha + \beta\gamma(1+\alpha)\frac{m_t}{m}\frac{\hat\omega}{\gamma} - (\beta\gamma)^2\frac{Q^{\mathrm{T,L}}(\hat\omega)}{\gamma^2}\right]\right.$$
$$\left.\times(\beta\gamma)^{\alpha+1}\Gamma(-\alpha-1,\beta\gamma) - \left[\alpha - \beta\gamma\left(1-\frac{m_t}{m}\frac{\hat\omega}{\gamma}\right)\right]\mathrm{e}^{-\beta\gamma}\right\}, \tag{2.8}$$

where $\hat\omega := \omega/m_t$ and

$$Q^{\mathrm{T,L}}(\hat{\omega}) := (1+\hat{\omega}^2)\Delta^{\mathrm{T,L}} + \frac{1}{4}\frac{m_{\mathrm{t}}^2}{m^2}, \tag{2.9}$$

with $\Delta^{\mathrm{T,L}}$ in (2.2).

The spectral range of the radiation densities (2.1) is $0 < \omega < \omega_{\max}(\gamma)$, cf. (2.3). Inversely, the condition $\omega_{\max}(\hat{\gamma}) - \omega = 0$ or

$$\hat{\gamma}(\omega) = \mu\sqrt{1+\hat{\omega}^2} + \frac{1}{2}\frac{m_{\mathrm{t}}}{m}\hat{\omega} \tag{2.10}$$

defines the minimal electronic Lorentz factor for radiation at this frequency. ($\hat{\omega}$ stands for the rescaled frequency ω/m_{t}.) That is, an electron in uniform motion can radiate at ω only if its Lorentz factor exceeds $\hat{\gamma}(\omega)$. The lower edge of Lorentz factors in the electron distribution defines the break frequency, $\omega_1 := \omega_{\max}(\gamma_1)$, or

$$\frac{\omega_1}{m_{\mathrm{t}}} = \mu\sqrt{\gamma_1^2 - 1} - \frac{1}{2}\frac{m_{\mathrm{t}}}{m}\gamma_1, \tag{2.11}$$

which separates the spectrum into a low- and high-frequency band. We have $\hat{\gamma}(\omega_1) = \gamma_1$, and $\hat{\gamma}(\omega) > \gamma_1$ if $\omega > \omega_1$; $\gamma_1 = \mu$ corresponds to $\omega_1 = 0$. The averaged energy density (2.6) can be assembled as

$$\begin{aligned}\langle p^{\mathrm{T,L}}(\omega;\gamma_1,n_1)\rangle_{\alpha,\beta} = A_{\alpha,\beta}(\gamma_1,n_1)\big[&B^{\mathrm{T,L}}(\omega;\gamma_1;\alpha,\beta)\theta(\omega_1-\omega)\\ &+B^{\mathrm{T,L}}(\omega;\hat{\gamma}(\omega);\alpha,\beta)\theta(\omega-\omega_1)\big],\end{aligned} \tag{2.12}$$

with $\hat{\gamma}(\omega)$ in (2.10). The superscripts T and L denote the transversal and longitudinal polarization components, $\langle p^{\mathrm{T}}\rangle_{\alpha,\beta}$ is the energy transversally radiated per unit time and unit frequency.

3. Tachyonic spectral averages and spectral fits

To get an overview of the averaged spectral densities (2.12), we consider their asymptotic limits. The low-temperature expansion, $\beta \gg 1$, is readily found by substituting the asymptotic expansion of the incomplete Γ-function [21] into the spectral function $B^{\mathrm{T,L}}(\omega;\gamma;\alpha,\beta)$, cf. (2.8),

$$B^{\mathrm{T,L}}(\omega;\gamma;\alpha,\beta) \sim \frac{\alpha_{\mathrm{q}} m_{\mathrm{t}}\hat{\omega}}{1+\hat{\omega}^2}\frac{\mathrm{e}^{-\beta\gamma}}{\gamma^\alpha\beta}\left[C_0^{\mathrm{T,L}}(\gamma) + \frac{C_1^{\mathrm{T,L}}(\gamma)}{\beta\gamma} + \cdots\right], \tag{3.1}$$

where

$$\begin{aligned} C_0^{\mathrm{T,L}}(\gamma) &:= 1 - \frac{m_{\mathrm{t}}}{m}\frac{\hat{\omega}}{\gamma} - \frac{Q^{\mathrm{T,L}}(\hat{\omega})}{\gamma^2},\\ C_1^{\mathrm{T,L}}(\gamma) &:= -\alpha + (1+\alpha)\frac{m_{\mathrm{t}}}{m}\frac{\hat{\omega}}{\gamma} + (2+\alpha)\frac{Q^{\mathrm{T,L}}(\hat{\omega})}{\gamma^2}. \end{aligned} \tag{3.2}$$

This holds for Lorentz factors $\gamma \geqslant \mu$, cf. after (2.5), $Q^{\mathrm{T,L}}(\hat{\omega})$ is defined in (2.9), and the expansion parameter is $\beta\gamma \gg 1$.

The high-temperature expansion, $\beta \ll 1$, of $B^{\mathrm{T,L}}$ is obtained by substituting the ascending series [21]

$$(\beta\gamma)^{\alpha+1}\Gamma(-\alpha-1,\beta\gamma) = (\beta\gamma)^{\alpha+1}\Gamma(-\alpha-1) + \frac{1}{\alpha+1} - \frac{\beta\gamma}{\alpha} + \frac{(\beta\gamma)^2}{2!(\alpha-1)} - \cdots \tag{3.3}$$

The expansion applicable for $\beta\gamma \ll 1$ is thus

$$B^{\mathrm{T,L}}(\omega;\gamma;\alpha,\beta) = \frac{\alpha_{\mathrm{q}} m_{\mathrm{t}}\hat{\omega}}{1+\hat{\omega}^2}\gamma^{1-\alpha}\Bigg\{(\beta\gamma)^{\alpha-1}\Gamma(-\alpha-1)\Bigg[(1+\alpha)\alpha+\beta\gamma(1+\alpha)\frac{m_{\mathrm{t}}}{m}\frac{\hat{\omega}}{\gamma} - (\beta\gamma)^2\frac{Q^{\mathrm{T,L}}(\hat{\omega})}{\gamma^2}\Bigg] + \sum_{k=0}^{\infty}\frac{(-)^k}{k!}(\beta\gamma)^k D_k^{\mathrm{T,L}}(\hat{\omega};\gamma,\alpha)\Bigg\}, \tag{3.4}$$

with the shortcut

$$D_k^{\mathrm{T,L}}(\hat{\omega};\gamma,\alpha) := \frac{1}{\alpha-k-1} - \frac{m_{\mathrm{t}}}{m}\frac{\hat{\omega}}{\gamma}\frac{1}{\alpha-k} - \frac{Q^{\mathrm{T,L}}(\hat{\omega})}{\gamma^2}\frac{1}{\alpha-k+1}. \tag{3.5}$$

In the opposite limit, $\beta\gamma \gg 1$, we may still use the low-temperature expansion (3.1), even if $\beta \ll 1$. Singularities occurring at integer α in (3.4) and (3.5) cancel if ε-expanded. To this end, we substitute $\alpha = n - \varepsilon$ as well as the ε-expansion of the Γ-function at its poles,

$$\begin{aligned}&\Gamma(-n+\varepsilon) = \frac{(-)^n}{n!}\left(\frac{1}{\varepsilon}+\psi(n+1)+\mathrm{O}(\varepsilon)\right),\\ &\psi(n+1) = -\gamma_{\mathrm{E}} + 1 + \frac{1}{2} + \cdots + \frac{1}{n}, \quad \psi(1) = -\gamma_{\mathrm{E}},\end{aligned} \tag{3.6}$$

valid for $n \geqslant 0$. At $\alpha = n \geqslant 1$, we obtain

$$\begin{aligned}B^{\mathrm{T,L}}(\omega;\gamma;n,\beta) = \frac{\alpha_{\mathrm{q}} m_{\mathrm{t}}\hat{\omega}}{1+\hat{\omega}^2}\gamma^{1-n}\Bigg\{&\sum_{\substack{k=0\\ k\neq n-1,n,n+1}}^{\infty}\frac{(-)^k}{k!}(\beta\gamma)^k D_k^{\mathrm{T,L}}(\hat{\omega};\gamma,n)\\ &-\frac{(-)^{n-1}}{(n-1)!}(\beta\gamma)^{n-1}\left[\log(\beta\gamma)-\psi(n)+\frac{1}{2}\frac{Q^{\mathrm{T,L}}(\hat{\omega})}{\gamma^2}+\frac{m_{\mathrm{t}}}{m}\frac{\hat{\omega}}{\gamma}\right]\\ &-\frac{(-)^n}{n!}(\beta\gamma)^n\left[1+\frac{Q^{\mathrm{T,L}}(\hat{\omega})}{\gamma^2}-\frac{m_{\mathrm{t}}}{m}\frac{\hat{\omega}}{\gamma}(\log(\beta\gamma)-\psi(n+1))\right]\\ &-\frac{(-)^{n+1}}{(n+1)!}(\beta\gamma)^{n+1}\left[\frac{1}{2}-\frac{Q^{\mathrm{T,L}}(\hat{\omega})}{\gamma^2}(\log(\beta\gamma)-\psi(n+2))-\frac{m_{\mathrm{t}}}{m}\frac{\hat{\omega}}{\gamma}\right]\Bigg\}.\end{aligned} \tag{3.7}$$

At $\alpha = 0$, we find

$$\begin{aligned}B^{\mathrm{T,L}}(\omega;\gamma;0,\beta) = \frac{\alpha_{\mathrm{q}} m_{\mathrm{t}}\hat{\omega}}{1+\hat{\omega}^2}\gamma\Bigg\{&\frac{1}{\beta\gamma}-\left[1+\frac{Q^{\mathrm{T,L}}(\hat{\omega})}{\gamma^2}-\frac{m_{\mathrm{t}}}{m}\frac{\hat{\omega}}{\gamma}(\log(\beta\gamma)-\psi(1))\right]\\ &+\beta\gamma\left[\frac{1}{2}-\frac{Q^{\mathrm{T,L}}(\hat{\omega})}{\gamma^2}(\log(\beta\gamma)-\psi(2))-\frac{m_{\mathrm{t}}}{m}\frac{\hat{\omega}}{\gamma}\right]\\ &+\sum_{k=2}^{\infty}\frac{(-)^k}{k!}(\beta\gamma)^k D_k^{\mathrm{T,L}}(\hat{\omega};\gamma,0)\Bigg\},\end{aligned} \tag{3.8}$$

and at $\alpha = -1$,

$$B^{\mathrm{T,L}}(\omega;\gamma;-1,\beta)=\frac{\alpha_{\mathrm{q}}m_{\mathrm{t}}\hat{\omega}}{1+\hat{\omega}^2}\gamma^2\left\{\frac{1}{(\beta\gamma)^2}-\frac{1}{\beta\gamma}\frac{m_{\mathrm{t}}}{m}\frac{\hat{\omega}}{\gamma}-\left[\frac{1}{2}-\frac{Q^{\mathrm{T,L}}(\hat{\omega})}{\gamma^2}(\log(\beta\gamma)-\psi(1))-\frac{m_{\mathrm{t}}}{m}\frac{\hat{\omega}}{\gamma}\right]\right.$$
$$\left.+\sum_{k=1}^{\infty}\frac{(-)^k}{k!}(\beta\gamma)^k D_k^{\mathrm{T,L}}(\hat{\omega};\gamma,-1)\right\}. \tag{3.9}$$

There are no singularities in (3.4) for $\alpha\leqslant -2$.

If $\gamma_1=\mu$, $\beta\ll 1$ and $\alpha>1$, the maximum of $\langle p^{\mathrm{T,L}}(\omega;\gamma_1,n_1)\rangle_{\alpha,\beta}$, cf. (2.12), is determined by the leading factor $\propto\omega\hat{\gamma}^{-\alpha-1}$ in the high-temperature expansion (3.4). This peak is located at $\omega_{\max}\approx m_{\mathrm{t}}/\sqrt{\alpha}$ and is followed by power-law decay $\propto\omega^{-\alpha}$ for $\omega\ll m_{\mathrm{t}}/\beta$ and exponential decay starting at about $\omega\approx m_{\mathrm{t}}/\beta$. The low-temperature expansion (3.1) applies for $\omega\gg m_{\mathrm{t}}/\beta$. If $\gamma_1\gg 1$ (but still $\beta\gamma_1\ll 1$ and $\alpha>1$), the peak of $\langle p^{\mathrm{T,L}}(\omega;\gamma_1,n_1)\rangle_{\alpha,\beta}$ is determined by the factor $\omega/(\omega^2+m_{\mathrm{t}}^2)$ in (3.4) and occurs at $\omega_{\max}\approx m_{\mathrm{t}}$. It is followed by a broken power-law, at first $\langle p^{\mathrm{T,L}}\rangle_{\alpha,\beta}\propto 1/\omega$ in the range $1\ll\omega/m_{\mathrm{t}}\ll\gamma_1$ and then $\langle p^{\mathrm{T,L}}\rangle_{\alpha,\beta}\propto\omega^{-\alpha}$ in the interval $\gamma_1\ll\omega/m_{\mathrm{t}}\ll 1/\beta$. At $\omega\approx m_{\mathrm{t}}/\beta$, there is an exponential cutoff according to (3.1).

The spectral fits in Figs. 1–6 are performed with the E^2-rescaled flux density $E^2\mathrm{d}N^{\mathrm{T,L}}/\mathrm{d}E$, which relates to the energy density $\langle p^{\mathrm{T,L}}\rangle_{\alpha,\beta}$ in (2.12) as

$$E^2\frac{\mathrm{d}N^{\mathrm{T,L}}(E;\alpha,\beta,\gamma_1,n_1)}{\mathrm{d}E}:=\frac{\omega}{4\pi d^2}\langle p^{\mathrm{T,L}}(\omega;\gamma_1,n_1)\rangle_{\alpha,\beta}, \tag{3.10}$$

where d is the distance to the source. The preceding scaling relations for $\langle p^{\mathrm{T,L}}\rangle_{\alpha,\beta}$ give a plateau value $E^2\mathrm{d}N^{\mathrm{T,L}}/\mathrm{d}E\propto 1$ in the range $1\ll E/(m_{\mathrm{t}}c^2)\ll\gamma_1$, followed by power-law

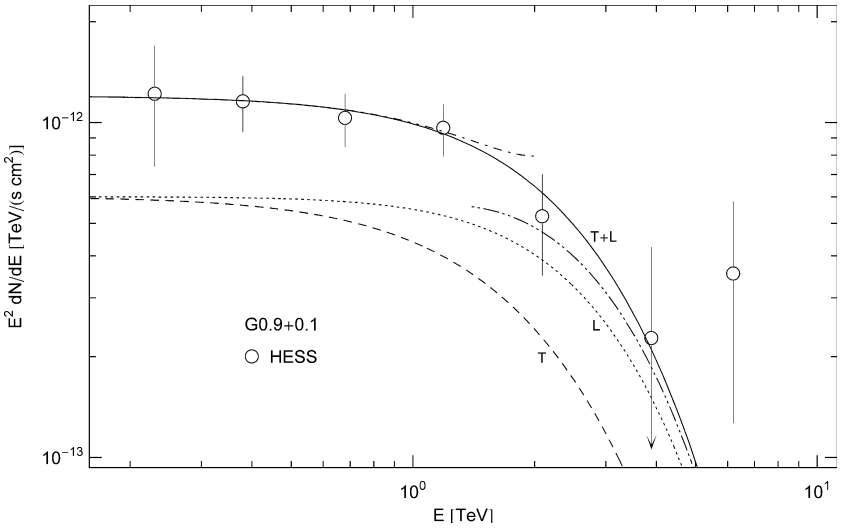

Fig. 1. Spectral map of the pulsar wind nebula in SNR G0.9+0.1. Data points from HESS [22]. The solid line T+L depicts the unpolarized differential tachyon flux $\mathrm{d}N^{\mathrm{T+L}}/\mathrm{d}E$, rescaled with E^2 for better visibility of the spectral curvature, cf. (3.10). The transversal (T, dashed) and longitudinal (L, dotted) flux densities $dN^{\mathrm{T,L}}/\mathrm{d}E$ add up to the total flux T + L. The high-temperature/low-frequency approximation (dot-dashed) of T + L is based on the first two orders of the ascending series in (3.4), the low-temperature/high-frequency asymptotics (dot-dot-dashed) is calculated from the two leading orders in (3.1). The unpolarized flux T + L is the actual spectral fit, the parameters of the electron density are recorded in Table 1.

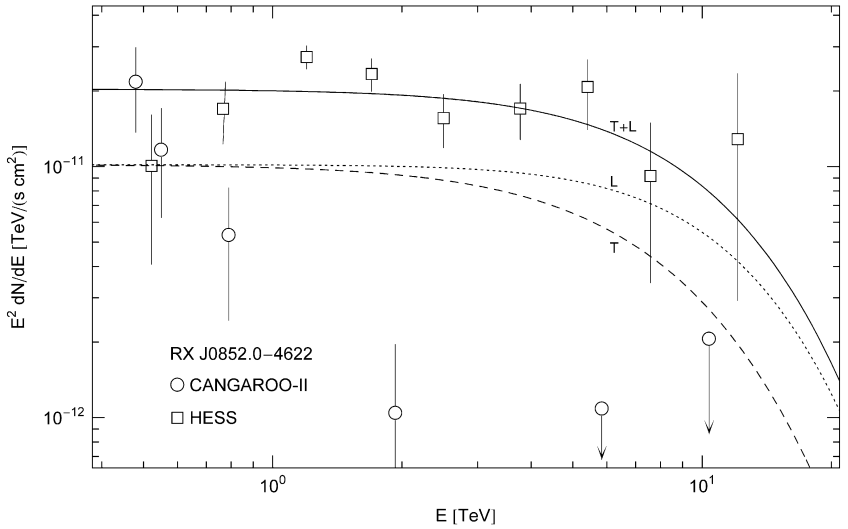

Fig. 2. Spectral map of SNR RX J0852.0−4622, data points from CANGAROO-II [25] and HESS [26]. The plots are labeled as in Fig. 1. T and L stand for the transversal and longitudinal flux components, and T+L labels the total unpolarized flux. Only the first two CANGAROO-II points (above the 10^{-11}-mark) have been taken into account in the spectral fit. The CANGAROO and HESS data sets define different slopes, the CANGAROO slope is much steeper. γ-Ray observations of the Galactic center [27,28] also resulted in diverging slopes, cf. Fig. 4 in [28]. The HESS points and the two overlapping CANGAROO points define an extended spectral plateau in the high GeV range typical for cascade spectra, which is followed by exponential decay. The parameters of the inferred thermal electron density are listed in Table 1.

decay $E^2\mathrm{d}N^{\mathrm{T,L}}/\mathrm{d}E \propto E^{1-\alpha}$ in the band $\gamma_1 \ll E/(m_\mathrm{t}c^2) \ll 1/\beta$, and subsequent exponential decay.

In the foregoing discussion of the high-temperature asymptotics, we assumed an electron index $\alpha > 1$. We still have to settle the case $\alpha < 1$. The spectral peak at $\omega_{\max} \approx m_\mathrm{t}$ is again determined by the factor $\omega/(\omega^2 + m_\mathrm{t}^2)$. Adjacent is a power-law slope $\langle p^{\mathrm{T,L}} \rangle_{\alpha,\beta} \propto 1/\omega$ in the range $1 \ll \omega/m_\mathrm{t} \ll 1/\beta$, so that $E^2\mathrm{d}N^{\mathrm{T,L}}/\mathrm{d}E \propto 1$, cf. (3.10). At $\omega \approx m_\mathrm{t}/\beta$, there is the cross-over to exponential decay, cf. (3.1). This holds true for $\gamma_1 = \mu$, cf. (2.3), as well as $\gamma_1 \gg 1$, provided $\beta\gamma_1 \ll 1$, since the leading order of (3.4) does not depend on γ for $\alpha < 1$. If $\beta\gamma_1 \gg 1$ despite β being small, then the low-temperature expansion (3.1) applies instead of (3.4).

As the polarization is not observed, we add the transversal and longitudinal densities, writing $\langle p^{\mathrm{T+L}} \rangle := \langle p^{\mathrm{T}} \rangle + \langle p^{\mathrm{L}} \rangle$ for the energy density and $N^{\mathrm{T+L}} := N^{\mathrm{T}} + N^{\mathrm{L}}$ for the number flux, the spectral fits in Figs. 1–6 are based on the unpolarized differential flux, $\mathrm{d}N^{\mathrm{T+L}}/\mathrm{d}E$, defined in (3.10). We restore the natural units on the right-hand side of (3.10), up to now we have used $\hbar = c = 1$, and write $E_{(1)}$ for $\hbar\omega_{(1)}$; the plots in Figs. 1–6 are in TeV units, with $\mathrm{d}N^{\mathrm{T,L}}/\mathrm{d}E$ in units of $\mathrm{TeV}^{-1}\mathrm{s}^{-1}\mathrm{cm}^{-2}$. The normalization factor in (2.12) is dimensionless, $A_{\alpha,\beta} = n_1/\int_{\gamma_1}^{\infty} \mathrm{d}\rho_{\alpha,\beta}(\gamma)$, where n_1 is the number of radiating electrons with Lorentz factors exceeding γ_1, distributed according to density $\mathrm{d}\rho_{\alpha,\beta}$ in (2.5). α is the electronic power-law index, and β the exponential cutoff in the electron spectrum, both to be determined from the spectral fit like n_1 and γ_1. As for the electron count n_1, it is convenient to use a rescaled parameter $\hat{n}_1$ for the fit,

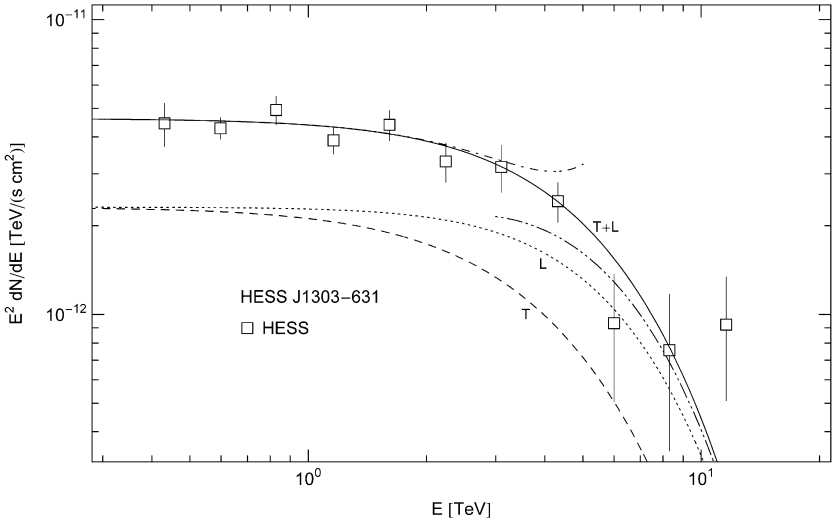

Fig. 3. Spectral map of the extended TeV γ-ray source HESS J1303−631. Data points from HESS [35]. The unpolarized spectral fit T + L is based on the electron density in Table 1, the polarized flux components are labeled T and L. The high- and low-temperature approximations of T + L are indicated by truncated dot-dashed and double-dot-dashed curves, respectively, with cross-over in the low TeV range. The electron populations producing the spectra in Figs. 1–3 are thermal, the electron temperature is of the same order in all three sources, cf. Table 1. The spectral curvature is generated by the Boltzmann factor, cf. (3.1), the GeV plateau terminates in exponential decay without a power-law cross-over.

$$\hat{n}_1 := \frac{\alpha_q n_1}{\hbar[\mathrm{keV\ s}]\ 4\pi d^2[\mathrm{cm}]} \approx 1.27\times 10^{-39}\frac{n_1}{d^2[\mathrm{kpc}]}, \tag{3.11}$$

which determines the amplitude of the tachyon flux. Here, $\hbar$[keV s] implies the tachyon mass in keV units, that is, we put $m_t c^2 \approx 2.15$ in the spectral function (2.8). The tachyon–electron mass ratio is $m_t/m \approx 1/238$, cf. after (2.3). The fitting procedure and in particular the spectral maps in Figs. 1–6 are not affected by the often uncertain distance estimate, in contrast to the source count, cf. Table 1.

Fig. 1 shows the high-energy spectral map of the composite SNR G0.9+0.1 [22–24] in the Galactic center, at a distance of 10 kpc [23,24]. The core component is presumably a pulsar wind nebula, though no pulsed emission has yet been detected.

In Fig. 2, we show the tachyonic spectral map of the shell-type SNR RX J0852.0−4622 [25–34]. The 1.157 MeV line of the short-lived ^{44}Ti isotope (with a half-life of 60 yr) was detected by COMPTEL, and an age of 700 years and a distance of 0.2 kpc was inferred [29,30,34]. This detection, however, was marginal [32], and column density estimates suggest a distance of 1–2 kpc, in the direction of and probably associated with the Vela Molecular Ridge [30]. A compact X-ray source has been located near the SNR center [32,33].

The spectrum of the extended TeV source HESS J1303−631 [35] is depicted in Fig. 3. The distance of 15.8 kpc is inferred from an association with PSR J1301−6305 [36], but could be one order smaller, since associations with other pulsars or molecular clouds at much smaller distance are possible [35].

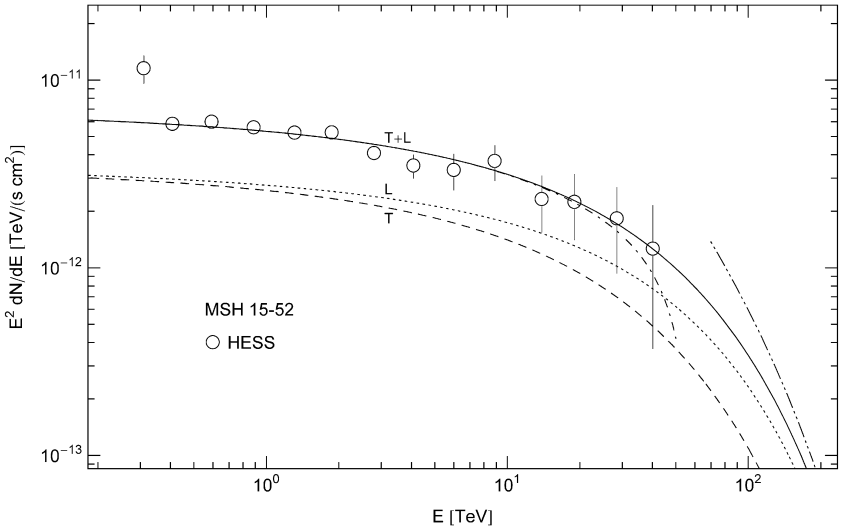

Fig. 4. Spectral map of the pulsar wind nebula in MSH 15-52. Data points from HESS [37]. The tachyonic spectral fit (solid line T+L) is obtained with a non-thermal electron distribution, cf. Table 1. The fit is for unpolarized radiation and can be split into a transversally (T) and longitudinally (L) polarized flux. The cutoff frequency of the averaged radiation densities (T, L and T+L) is $E_{\rm cut} = (m_{\rm t}/m)kT \approx 70$ TeV, defined by $\hat{\gamma}(\omega_{\rm cut}) = 1/\beta$ according to the low-temperature/high-frequency expansion (3.1). The high- and low-temperature asymptotics of the unpolarized total flux T+L is depicted by the dot-dashed and dot-dot-dashed curves. Most of the data points lie in the high-temperature/low-frequency regime, contrary to Figs. 1–3. The decay in this regime is gradual but not power-law, with electron index $\alpha < 1$, cf. the discussion following (3.10).

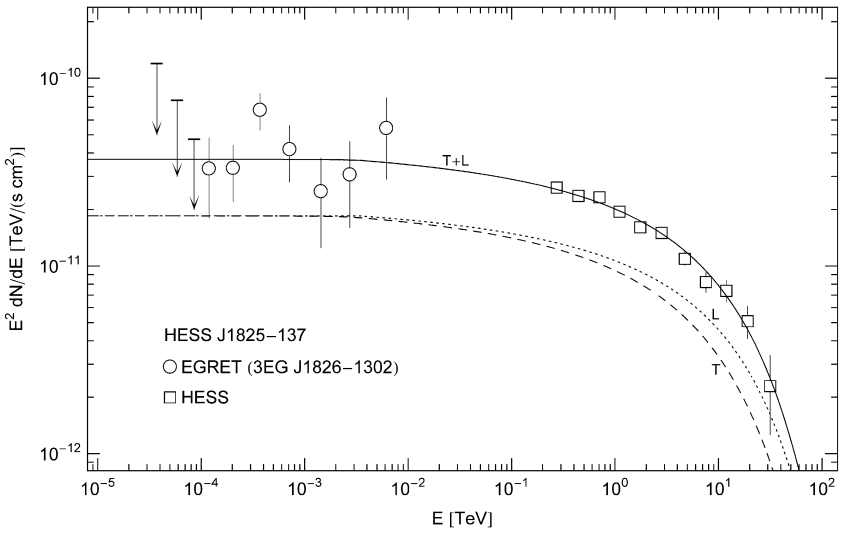

Fig. 5. Combined spectral map of the EGRET source 3EG J1826−1302 and the TeV source HESS J1825−137. Data points from EGRET [42] and HESS [41]. The solid line T+L is the spectral fit, T and L are the polarization components of the tachyon flux generated by a non-thermal electron density, cf. Table 1. The spectral break at $E \approx m_{\rm t}\gamma_1 \approx 3.4$ GeV is barely visible as edge in the spectral map, cf. after (3.10), followed by exponential decay with electron index $\alpha \approx 0.8$ and cutoff frequency $E_{\rm cut} \approx 40$ TeV.

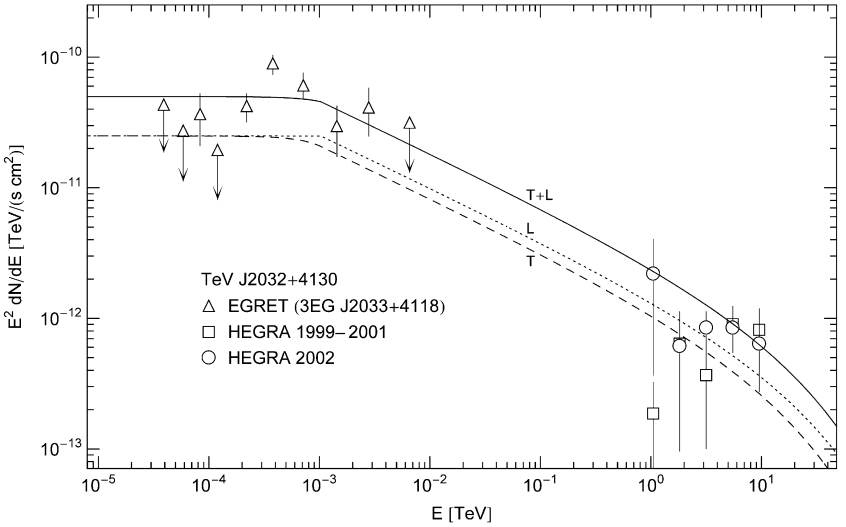

Fig. 6. Combined spectral map of the EGRET source 3EG J2033+4118 and the TeV source TeV J2032+4130. Data points from EGRET [42] and HEGRA [46]. A non-thermal electron population listed in Table 1 is inferred from the spectral fit T+L, obtained by adding the polarization components T and L. As the electron index exceeds 1, there emerges a power-law slope $\propto E^{1-\alpha}$, $\alpha \approx 1.4$, separating the GeV plateau from exponential decay. The spectral break between GeV plateau and power-law slope occurs at $m_t\gamma_1 \approx 1.0$ GeV, cf. Table 1. The slope is nearly straight, the cutoff temperature of the electron density is too high ($E_{\rm cut} \approx 160$ TeV) to significantly curve the slope in the range covered by the TeV data points.

Table 1
Electronic source densities generating the tachyonic spectral maps of the supernova remnants and TeV γ-ray sources in Figs. 1–6

	α	β	γ_1	$\hat{n}_1$	d (kpc)	$n^{\rm e}/d^2$ (kpc)	kT (TeV)
G0.9+0.1	−2	2.15×10^{-9}	μ	1.3×10^{-4}	10	7.5×10^{45}	240
RX J0852.0−4622	−2	5.38×10^{-10}	μ	2.2×10^{-3}	2	1.3×10^{47}	950
HESS J1303−631	−2	1.02×10^{-9}	μ	5.0×10^{-4}	15.8	2.9×10^{46}	500
MSH 15-52	0.6	3.07×10^{-11}	μ	7.5×10^{-4}	4.4	4.3×10^{46}	1.7×10^{4}
HESS J1825−137	0.8	5.38×10^{-11}	1.6×10^{6}	4.0×10^{-3}	4.1	2.3×10^{47}	9.5×10^{3}
TeV J2032+4130	1.4	1.34×10^{-11}	4.8×10^{5}	5.4×10^{-3}	15	3.1×10^{47}	3.8×10^{4}

The electron densities $\mathrm{d}\rho_{\alpha,\beta}$ in (2.5) are defined by parameters (α, β, γ_1, $\hat{n}_1$) extracted from the spectral fit. α is the electronic power-law index and β the cutoff parameter in the Boltzmann factor. The lower edge of electronic Lorentz factors in the source population is identified with the radiation threshold, $\gamma_1 = \mu$, cf. (2.3), except for HESS J1825−137 and TeV J2032+4130. $\hat{n}_1$ is the amplitude of the tachyonic flux density, from which the electron count $n^{\rm e}$ is inferred, cf. (3.11). d is the distance to the source, and kT the electron temperature. The high-energy spectra of the SNRs G0.9+0.1 and RX J0852.0−4622 as well as the extended TeV source HESS J1303−631 are thermal, $\alpha = -2$. The spectra of the pulsar wind nebula MSH 15-52 and the TeV sources HESS J1825−137 and TeV J2032+4130 are power-law with exponential cutoff. The distance estimates do not affect the spectral maps in Figs. 1–6 but the electronic source count $n^{\rm e}$. The distances of RX J0852.0−4622, HESS J1303−631 and TeV J2032+4130 could be one order lower than the listed ones, references are given after (3.11).

In Fig. 4, we plot the spectral map of the pulsar wind nebula in MSH 15-52 [37–40]. The nebula is powered by PSR B1509−58 [38,39], located at a distance of 4.4 kpc [40].

The spectrum of the TeV source HESS J1825−137 [41–44] is shown in Fig. 5. This source is associated with the EGRET source 3EG J1826−1302 [41], which is believed to be powered by PSR B1823−13 [43]. A further association of this pulsar with HESS J1825−137 is suggested by the one-sided X-ray morphology of the asymmetric pulsar wind nebula G18.0−0.7 powered by PSR B1823−13 [44], since the TeV emission of HESS J1825−137 is likewise strongly one-sided [41]. The distance estimate for PSR B1823−13 is 4.1 kpc [40].

Fig. 6 shows the spectral map of the presumably extended TeV source TeV J2032+4130 [45–48], associated with the EGRET source 3EG J2033+4118 [45]. The distance estimate is 15 kpc, inferred from an association with the low-mass X-ray binary 4U 1624–49 [47,48]. However, TeV J2032+4130 could be as close as 1.7 kpc if located in the Cyg OB2 association [45,46].

Once $\hat{n}_1$ is extracted from the spectral fit, we calculate via (3.11) the number of radiating electrons n_1 constituting the density $\mathrm{d}\rho_{\alpha,\beta}$. This, however, implies that all tachyons reaching the detector are properly counted. At γ-ray energies, only a tiny α_q/α_e-fraction (the ratio of tachyonic and electric fine structure constants, $\alpha_q/\alpha_e \approx 1.4\times 10^{-11}$) of the tachyon flux is actually absorbed [49,50]. This requires a rescaling of the electron count n_1, so that the actual number of radiating electrons is $n^e := n_1\alpha_e/\alpha_q \approx 7.3\times 10^{10}\ n_1$. (This rescaling applies to γ-ray spectra only, to frequencies much higher than the 2 keV tachyon mass, so that the mass-square can be dropped in the tachyonic dispersion relation. At X-ray energies, we have to rescale with the respective cross-section ratio, $\sigma_e(\omega)/\sigma_q\ (\omega)$, where σ_e is the electromagnetic cross-section and σ_q its tachyonic counterpart [7].) In Table 1, we list the flux amplitude $\hat{n}_1$ inferred from the spectral fit, as well as the renormalized electron count n^e depending on the distance estimate. The density $\mathrm{d}\rho_{\alpha,\beta}$ is defined by parameters $(\alpha,\beta,\gamma_1,\hat{n}_1\to n_1\to n^e)$ obtained from the spectral fit. For instance, the source count in the surface field of PSR B1509−58 is $n^e \approx 1.3\times 10^{47}$ [49], to be compared to 8.3×10^{47} obtained here for the pulsar wind nebula in MSH 15-52, cf. Table 1.

4. Conclusion

We have studied superluminal radiation from electrons in uniform motion. Tachyonic synchrotron and cyclotron radiation were investigated in [17]. In the zero-magnetic-field limit, the tachyonic synchrotron densities converge to the spectral densities (2.1) for uniform motion. Orbital curvature induces modulations in the spectral densities. At μG-field strengths as encountered in the shock-heated plasmas of SNRs, these oscillations are quite small, just tiny ripples along the slope of densities (2.1) with increasing amplitude toward the spectral break. If integrated over a thermal or power-law electron population, the oscillations are averaged out, so that the spectral densities (2.12) can still be used for electron trajectories bent by weak magnetic fields. As discussed in the Introduction, the source particles radiate in uniform motion, there is no electromagnetic radiation damping unless the trajectories spiral through magnetic fields. The energy radiated is drained from the absorber breaking the time symmetry of the Green function outside the lightcone.

We averaged the superluminal flux densities with electronic source distributions, derived the high- and low-temperature expansions of the spectral averages, and explained the spectral plateaus, the power-law slopes and the curvature of the spectral maps. We demonstrated that the γ-ray spectra of the supernova remnants and TeV sources listed in Table 1 can be reproduced by tachyonic cascade spectra. Speed and energy of tachyonic

quanta are related by $\hbar\omega = m_{\mathrm{t}}c^2(v^2/c^2 - 1)^{-1/2}$. At γ-ray energies, their speed is close to the speed of light, the basic difference to electromagnetic radiation is the longitudinally polarized flux component. The polarization of tachyons can be determined from transversal and longitudinal ionization cross-sections, which peak at different scattering angles [51].

The source numbers listed in Table 1 are lower bounds based on γ-ray emission only. The tachyonic fine structure constant enters as a square in the number count, once via (3.11) when inferring the preliminary count n_1 from the spectral fit, and a second time when rescaling this count to obtain the actual source number n_1^{e}. The tachyonic fine structure constant is an independent estimate from Lamb shifts in hydrogenic ions [5], it enters only linearly in the spectral density (2.1), in contrast to the squared electromagnetic constant in the Klein–Nishina cross section. The cutoff in the electron energy is much higher compared to a Compton fit, which compensates the small tachyonic fine structure constant in the spectral density and the absorption probability, as well as the reduced source count.

Source counts based on Compton fits have not yet been calculated for the sources discussed here, but one can obtain a rough estimate if one considers the Compton count for the Crab Nebula and rescales with the observed TeV power ratio. To this end, we use the total TeV flux of the respective source in Crab units, such as $F/F_{\mathrm{Crab}} \approx 0.02$ for SNR G0.9+0.1, cf. [22]. The flux of SNR RX J0852.0−4622 is roughly that of the Crab [26]. A flux ratio of 0.17 for HESS J1303−631 is quoted in [35], and a ratio of 0.15 for MSH 15-52 in [37]. The TeV flux of HESS J1825−137 is a 0.68 fraction of the Crab [41], and the flux collected from TeV J2032+4130 amounts to 5% of the Crab flux [46]. The power ratio is obtained as $P/P_{\mathrm{Crab}} \approx (d^2[\mathrm{kpc}]/4)F/F_{\mathrm{Crab}}$, with 2 kpc to the Crab. The distance estimates of the respective sources are listed in Table 1.

A count of $n_{\mathrm{Crab}} \approx 1.3 \times 10^{51}$ electrons/positrons in the Crab was derived from an electromagnetic inverse-Compton model in [52]. An estimate of the Compton count for the above sources is found by rescaling with the power ratio. We obtain $n_{\mathrm{Crab}}P/P_{\mathrm{Crab}} \approx 3.7 \times 10^{51}$ both for HESS J1825−137 and TeV J2032+4130 (based on the distance estimates in Table 1); the estimates for the other sources are similar within one order of magnitude. The counts based on the tachyonic cascade fits in Figs. 1–6 are two to three orders lower than the respective Compton count, cf. Table 1. In either case, the distance estimate enters as a square, which can lower the source count of RX J0852.0−4622, HESS J1303−631 and TeV J2032+4130 by two orders, cf. after (3.11).

Apart from the extended plateaus in the spectral maps, it is the high cutoff in the electron energy rather than the mildly reduced source count that distinguishes tachyonic cascade spectra from inverse-Compton fits and, for that matter, hadronic radiation models based on pion decay [53,54]. In the case of a thermal electron distribution, with electron index $\alpha = -2$, we may identify $kT[\mathrm{TeV}] \approx 5.11 \times 10^{-7}/\beta$, cf. (2.5). We use this definition of electron temperature also for other electron indices; kT is the energy at which the exponential decay of the electron density sets in, cf. the end of Appendix A. The TeV spectra discussed here show significant curvature, and we demonstrated that this curvature is reproduced by an exponentially cut power-law electron distribution. The exponential shows in the low-temperature/high-frequency expansion of the averaged spectral density, cf. (2.12) and (3.1), curving the spectral slopes in double-logarithmic plots. This curvature is intrinsic, there is no attenuation owing to infrared background photons, as tachyons do not interact with electromagnetic radiation fields. Besides, the sources discussed here are all Galactic; tachyonic spectral maps of TeV blazars are studied in [55]. The cutoff kT in the electron energy listed in Table 1 is to be compared to the spectral breaks in the cosmic-ray spectrum. These breaks occur at about

$10^{3.5}$, $10^{5.8}$ and 10^7 TeV, dubbed knee, second knee and ankle, respectively [56]. In MSH 15-52 as well as HESS J1825−137 and TeV J2032+4130, the cutoff happens between the first and second knee. As for protonic source particles, the cutoff energies kT in Table 1 have to be multiplied with 1.8×10^3, the proton/electron mass ratio, so that we arrive beyond the ankle, at protons in the 10^{21} eV range, which suggests Galactic TeV γ-ray sources as production sites of ultra-high-energy cosmic rays. In this case, the tachyon/electron mass ratio in the spectral densities has to be replaced by $m_\mathrm{t}/m_\mathrm{p}\approx 2.3\times 10^{-6}$, cf.((2.1)–(2.11)). In Figs. 1–6, however, this is not necessary, since even the tachyon/electron ratio is too small to noticeably affect the spectral maps.

Acknowledgments

The author acknowledges the support of the Japan Society for the Promotion of Science. The hospitality and stimulating atmosphere of the Centre for Nonlinear Dynamics, Bharathidasan University, Trichy, and the Institute of Mathematical Sciences, Chennai, are likewise gratefully acknowledged.

Appendix A. Asymptotic normalization of the electronic source densities

We derive the low- and high-temperature expansions of the normalization factors $A_{\alpha,\beta}(\gamma_1,n_1)$ of densities (2.5),

$$\begin{aligned} &A_{\alpha,\beta}(\gamma_1,n_1)=n_1/K_{\alpha,\beta}(\gamma_1),\\ &K_{\alpha,\beta}(\gamma_1)=\int_{\gamma_1}^{\infty}\sqrt{\gamma^2-1}\gamma^{-\alpha-1}\mathrm{e}^{-\beta\gamma}\,\mathrm{d}\gamma, \end{aligned} \tag{A.1}$$

where n_1 is the number of source particles with Lorentz factors in the range $\gamma_1\leqslant\gamma\leqslant\infty$.

A.1. Low-temperature expansion of $K_{\alpha,\beta}(\gamma_1)$

To obtain the low-temperature expansion of $K_{\alpha,\beta}(\gamma_1=1)$, we substitute $\gamma=x+1$ in the integrand of (A.1), and then expand in x except for the exponential. Using term-by-term integration (via Watson's Lemma), we readily find

$$K_{\alpha,\beta}(1)\sim\sqrt{\frac{\pi}{2}}\frac{\mathrm{e}^{-\beta}}{\beta^{3/2}}\left[1-\frac{1}{\beta}\frac{3}{2}\left(\alpha+\frac{3}{4}\right)+\frac{1}{\beta^2}\frac{15}{8}\left(\alpha^2+\frac{5}{2}\alpha+\frac{23}{16}\right)+\cdots\right]. \tag{A.2}$$

The low-temperature expansion of $K_{\alpha,\beta}(\gamma_1)$ for $\gamma_1>1$ is found by substituting $\gamma=(1+x\upsilon_1^2)\gamma_1$ into (A.1), where $\upsilon_1^2:=1-1/\gamma_1^2$. We then expand the integrand in ascending powers of x, leaving the exponential untouched, and use term-by-term integration,

$$\begin{aligned} &K_{\alpha,\beta}(\gamma_1)\sim\frac{\mathrm{e}^{-\beta\gamma_1}}{\beta}\gamma_1^{-\alpha}\upsilon_1\left[1+\frac{A}{\beta\gamma_1\upsilon_1^2}-\frac{B}{(\beta\gamma_1\upsilon_1^2)^2}+\cdots\right],\\ &A:=1-(1+\alpha)\upsilon_1^2,\quad B:=1+(1+2\alpha)\upsilon_1^2-(2+3\alpha+\alpha^2)\upsilon_1^4. \end{aligned} \tag{A.3}$$

This expansion apparently applies if $\beta\gamma_1\upsilon_1^2\gg 1$, and can also be used for small β (high-temperature limit) and large γ_1, as long as this condition is met. If β is large and γ_1 close to one so that $\beta\gamma_1\upsilon_1^2$ is small, we have to proceed differently,

$$K_{\alpha,\beta}(\gamma_1) = K_{\alpha,\beta}(1) - k_{\alpha,\beta}(\gamma_1),$$
$$k_{\alpha,\beta}(\gamma_1) := \int_1^{\gamma_1} \sqrt{\gamma^2-1}\gamma^{-\alpha-1}\mathrm{e}^{-\beta\gamma}\,\mathrm{d}\gamma, \tag{A.4}$$

with the asymptotic series $K_{\alpha,\beta}(1)$ in (A.2). As for $k_{\alpha,\beta}(\gamma_1)$, we write $\gamma = 1+\delta x$, where $\delta := \gamma_1 - 1$, and expand the integrand in an ascending series in x, except for the exponential. Term-by-term integration gives a power-series in δ,

$$k_{\alpha,\beta}(\gamma_1) = \sqrt{2\delta}\mathrm{e}^{-\beta}\left[g\left(\frac{3}{2},\beta\delta\right) - \left(\alpha+\frac{3}{4}\right)g\left(\frac{5}{2},\beta\delta\right)\delta + \frac{1}{2}\left(\alpha^2+\frac{5}{2}\alpha+\frac{23}{16}\right)g\left(\frac{7}{2},\beta\delta\right)\delta^2 + \mathrm{O}(\delta^3)\right], \tag{A.5}$$

where we use the shortcut

$$g(j,\beta\delta) := \frac{\Gamma(j)-\Gamma(j,\beta\delta)}{(\beta\delta)^j} = \sum_{k=0}^{\infty}\frac{(-)^k(\beta\delta)^k}{k!(j+k)}, \tag{A.6}$$

with positive half-integer j. This high-temperature expansion of $K_{\alpha,\beta}(\gamma_1)$, defined by (A.4) with series (A.2) and (A.5) substituted, is applicable if $\beta \gg 1$ and $\delta := \gamma_1 - 1 \ll 1$, so that $\beta\delta$ is small. If $\beta\delta$ is large, the expansion of $K_{\alpha,\beta}(\gamma_1)$ in (A.3) applies. As mentioned, series (A.3) can be used in the high-temperature regime, $\beta \ll 1$, provided $\beta\gamma_1 \gg 1$.

A.2. High-temperature expansion of $K_{\alpha,\beta}(\gamma_1)$

We write $K_{\alpha,\beta}(\gamma_1)$ in (A.1) as

$$K_{\alpha,\beta}(\gamma_1) = \int_{\gamma_1}^{\infty}\gamma^{-\alpha}\sqrt{1-\frac{1}{\gamma^2}}\mathrm{e}^{-\beta\gamma}\,\mathrm{d}\gamma, \tag{A.7}$$

assuming at first $\gamma_1 > 1$. We expand the root, the term-by-term integration is based on

$$\int_{\gamma_1}^{\infty}\gamma^{-a}\mathrm{e}^{-\beta\gamma}\,\mathrm{d}\gamma = \beta^{a-1}\Gamma(1-a,\beta\gamma_1), \tag{A.8}$$

where we put $a = \alpha + 2n$,

$$K_{\alpha,\beta}(\gamma_1) = \sum_{n=0}^{\infty}\binom{1/2}{n}(-)^n\beta^{\alpha+2n-1}\Gamma(1-\alpha-2n,\beta\gamma_1). \tag{A.9}$$

Here, we substitute the ascending series

$$(\beta\gamma_1)^{a-1}\Gamma(1-a,\beta\gamma_1) = (\beta\gamma_1)^{a-1}\Gamma(1-a) + \sum_{k=0}^{\infty}\frac{(\beta\gamma_1)^k(-)^k}{(a-1-k)k!}, \tag{A.10}$$

interchange the summations, and substitute

$$(-)^n\binom{1/2}{n} = -\frac{1}{2\sqrt{\pi}}\frac{\Gamma(n-1/2)}{n!}. \tag{A.11}$$

In this way, we find the ascending β-expansion of $K_{\alpha,\beta}(\gamma_1)$ as

$$K_{\alpha,\beta}(\gamma_1)=\sum_{k=0}^{\infty}(-)^k\binom{1/2}{k}\beta^{\alpha+2k-1}\Gamma(1-\alpha-2k)+f_{\alpha,\beta}(\gamma_1), \tag{A.12}$$

where

$$f_{\alpha,\beta}(\gamma_1):=\frac{1}{2\sqrt{\pi}}\sum_{k=0}^{\infty}\frac{(-)^k\beta^k}{k!}\sum_{n=0}^{\infty}\frac{\Gamma(n-1/2)}{n!}\frac{\gamma_1^{1-\alpha+k-2n}}{1-\alpha+k-2n}. \tag{A.13}$$

It remains to find a more tractable expression for $f_{\alpha,\beta}(\gamma_1)$. To this end, we return to the integral $k_{\alpha,\beta}(\gamma_1)$ in (A.4). Expanding the exponential, the term-by-term integration is effected by

$$\int_1^{\gamma}\gamma^{-b-1}\sqrt{\gamma^2-1}\,\mathrm{d}\gamma=\frac{\sqrt{\pi}}{4}\frac{\Gamma((b-1)/2)}{\Gamma((b+2)/2)}+\frac{\gamma^{1-b}}{1-b}{}_2F_1\left(-\frac{1}{2},\frac{b-1}{2};\frac{b+1}{2};\frac{1}{\gamma^2}\right). \tag{A.14}$$

We write $b=\alpha-k$, and find

$$k_{\alpha,\beta}(\gamma_1)=\frac{\sqrt{\pi}}{4}\sum_{k=0}^{\infty}\frac{(-)^k\beta^k}{k!}\frac{\Gamma((\alpha-k-1)/2)}{\Gamma((\alpha-k+2)/2)}-f_{\alpha,\beta}(\gamma_1), \tag{A.15}$$

$$f_{\alpha,\beta}(\gamma_1):=\sum_{k=0}^{\infty}\frac{(-)^k(\beta\gamma_1)^k}{k!}\frac{\gamma_1^{1-\alpha}}{\alpha-k-1}{}_2F_1\left(-\frac{1}{2},\frac{\alpha-k-1}{2};\frac{\alpha-k+1}{2};\frac{1}{\gamma_1^2}\right). \tag{A.16}$$

The series (A.16) is identical with (A.13), by virtue of

$${}_2F_1\left(-\frac{1}{2},\frac{b-1}{2};\frac{b+1}{2};\frac{1}{\gamma_1^2}\right)=\frac{1-b}{2\sqrt{\pi}}\sum_{n=0}^{\infty}\frac{\Gamma(n-1/2)}{(2n+b-1)n!}\frac{1}{\gamma_1^{2n}}. \tag{A.17}$$

We thus find

$$K_{\alpha,\beta}(\gamma_1)=K_{\alpha,\beta}(0)+f_{\alpha,\beta}(\gamma_1),\quad k_{\alpha,\beta}(\gamma_1)=k_{\alpha,\beta}(\infty)-f_{\alpha,\beta}(\gamma_1), \tag{A.18}$$

$$K_{\alpha,\beta}(1)=K_{\alpha,\beta}(0)+k_{\alpha,\beta}(\infty), \tag{A.19}$$

where series $K_{\alpha,\beta}(0)$ and $k_{\alpha,\beta}(\infty)$ read as

$$K_{\alpha,\beta}(0):=\beta^{\alpha-1}\left[\Gamma(1-\alpha)-\frac{\beta^2}{2}\Gamma(-1-\alpha)-\frac{\beta^4}{8}\Gamma(-3-\alpha)+\cdots\right], \tag{A.20}$$

$$k_{\alpha,\beta}(\infty):=\frac{\sqrt{\pi}}{4}\left[\frac{\Gamma((\alpha-1)/2)}{\Gamma((\alpha+2)/2)}-\beta\frac{\Gamma((\alpha-2)/2)}{\Gamma((\alpha+1)/2)}+\frac{\beta^2}{2!}\frac{\Gamma((\alpha-3)/2)}{\Gamma(\alpha/2)}+\cdots\right]. \tag{A.21}$$

The coefficients in (A.20) are those of the root in (A.7). The notation $K_{\alpha,\beta}(0)$ and $k_{\alpha,\beta}(\infty)$ symbolizes the respective integrals in (A.7) and (A.4), with the exponential or root formally expanded. The high-temperature expansion of $K_{\alpha,\beta}(\gamma_1)$, defined by (A.12) and (A.16), is efficient for $\beta\gamma_1\ll 1$, provided γ_1 is not too close to one. If $\beta\gamma_1\gg 1$, we use the expansion of $K_{\alpha,\beta}(\gamma_1)$ in (A.3) instead. The high-temperature expansion of $K_{\alpha,\beta}(1)$ is defined by ((A.19)–(A.21)). There are singularities for integer α, which cancel in every order if ε-expanded, cf. Appendix B.

If $\gamma_1\approx 1$, we use

$$K_{\alpha,\beta}(\gamma_1)=K_{\alpha,\beta}(1)-k_{\alpha,\beta}(\gamma_1), \tag{A.22}$$

with $K_{\alpha,\beta}(1)$ defined by series ((A.19)–(A.21)) and

$$k_{\alpha,\beta}(\gamma_1)=\frac{1}{3}\sum_{k=0}^{\infty}\frac{(-)^k\beta^k}{k!}(\gamma_1^2-1)^{3/2}{}_2F_1\left(\frac{3}{2},\frac{\alpha-k+2}{2};\frac{5}{2};1-\gamma_1^2\right). \tag{A.23}$$

This series is recovered from (A.15), by substituting into (A.16) the identity [21]

$${}_2F_1\left(-\frac{1}{2},\frac{b-1}{2};\frac{b+1}{2};\frac{1}{\gamma_1^2}\right)=\frac{\sqrt{\pi}}{2}\frac{\Gamma((b+1)/2)}{\Gamma((b+2)/2)}\gamma_1^{b-1} + \frac{1-b}{3}\gamma_1^{b-1}(\gamma_1^2-1)^{3/2}{}_2F_1\left(\frac{3}{2},\frac{b+2}{2};\frac{5}{2};1-\gamma_1^2\right), \tag{A.24}$$

with $b=\alpha-k$. The series (A.23) can also directly be obtained from (A.4); we expand the exponential and use the variable substitution $y=\gamma^2-1$ and the integral representation

$$\int_0^{\gamma_1^2-1}(1+y)^{-(b+2)/2}\sqrt{y}\,\mathrm{d}y=\tfrac{2}{3}(\gamma_1^2-1)^{3/2}{}_2F_1\left(\frac{3}{2},\frac{b+2}{2};\frac{5}{2};1-\gamma_1^2\right). \tag{A.25}$$

The calculation of $K_{\alpha,\beta}(\gamma_1)$ via (A.22) and (A.23) is efficient for γ_1 close to one, such as $\gamma_1=\mu$, cf. after (2.5).

We discuss the location of the peak of the densities $\mathrm{d}\rho_{\alpha,\beta}(\gamma)$ in (2.5). $\gamma_{\max}$ is determined as the $\gamma>1$ zero of $\gamma^3+(\alpha/\beta)\gamma^2-\gamma-(\alpha+1)/\beta=0$. We give only the leading orders and state the expansion parameters. If $\beta\gg1$, we find $\gamma_{\max}=1+1/(2\beta)+\mathrm{O}(\beta^{-2})$. If $\beta\ll1$ and $\alpha<0$, we find $\gamma_{\max}=-(\alpha/\beta)(1+\mathrm{O}(\beta^2/\alpha^3))$, from the third and second order. In leading order, the 'displacement law' $\beta\gamma_{\max}\approx$ const holds true; the expansion parameter is stated in the preceding O-term. If $\beta\ll1$ and $\alpha>0$, $\gamma_{\max}=\sqrt{(\alpha+1)/\alpha}(1+\mathrm{O}(\beta/\alpha^{3/2}))$, via the zeroth and second order; this peak is followed by a power-law slope $\gamma^{-\alpha}$, extending to $\gamma\approx1/\beta$. Finally, if $\beta\ll1$ and α very close to zero, we may still have $\beta/|\alpha|^{3/2}\gg1$, so that the indicated expansions break down. In this case, we find $\gamma_{\max}=\beta^{-1/3}(1+\mathrm{O}(\beta^{2/3},\alpha/\beta^{3/2}))$, from the zeroth and third order, where the O-term stands for a double series in the indicated parameters.

Appendix B. ε-expansion of the normalization factors $K_{\alpha,\beta}(\gamma_1)$ at integer electron index α

We need two ε-expansions of the Γ-function, that of $\Gamma(-n+\varepsilon)$ in (3.6) and

$$\Gamma\left(\frac{1}{2}-n+\varepsilon\right)=\Gamma\left(\frac{1}{2}-n\right)\left(1+\varepsilon\psi\left(\frac{1}{2}-n\right)+\ \mathrm{O}(\varepsilon^2)\right),$$
$$\psi\left(\frac{1}{2}\pm n\right)=-\gamma_{\mathrm{E}}-2\log2+2\left(1+\frac{1}{3}+\cdots+\frac{1}{2n-1}\right), \tag{B.1}$$

valid for $n\geqslant0$. At $n=0$, the series $2(1+1/3+\ldots)$ is dropped. We at first give the ε-expansion of $K_{\alpha,\beta}(1)$ in (A.19). To this end, we decompose

$$K_{\alpha,\beta}(1)=K_{\alpha,\beta}(0)+\kappa_1+\kappa_2 \tag{B.2}$$

into three series. $K_{\alpha,\beta}(0)$ is the series (A.20),

$$K_{\alpha,\beta}(0)=-\frac{1}{2\sqrt{\pi}}\sum_{n=0}^{\infty}\frac{\Gamma(n-1/2)}{n!}\Gamma(1-\alpha-2n)\beta^{\alpha+2n-1}, \tag{B.3}$$

and the series $\kappa_{1,2}$ read

$$\kappa_1 := \frac{\sqrt{\pi}}{4}\sum_{n=0}^{\infty}\frac{\Gamma((\alpha-2n-1)/2)}{\Gamma((\alpha-2n+2)/2)}\frac{\beta^{2n}}{(2n)!}, \tag{B.4}$$

$$\kappa_2 := -\frac{\sqrt{\pi}}{4}\sum_{n=0}^{\infty}\frac{\Gamma((\alpha-2n-2)/2)}{\Gamma((\alpha-2n+1)/2)}\frac{\beta^{2n+1}}{(2n+1)!}, \tag{B.5}$$

obtained by splitting $k_{\alpha,\beta}(\infty)=\kappa_1+\kappa_2$ in (A.21). We substitute $\alpha=m+\varepsilon$, where m is an integer at which the series become singular. We then expand in ε, making use of the ε-expansions of the Γ-function in (3.6) and (B.1). The ε-poles cancel if the series are added according to (B.2). The following expansions of $K_{\alpha,\beta}(0)$ and $\kappa_{1,2}$ are valid up to terms of $O(\varepsilon)$.

We start by expanding $K_{\alpha,\beta}(0)$ in (B.3). We put $\alpha=2k+\varepsilon$ and find, for $k\geqslant 1$,

$$K_{\alpha,\beta}(0) = -\frac{1}{2\sqrt{\pi}}\sum_{n=0}^{\infty}\frac{\beta^{2n+2k-1}}{(2n+2k-1)!}\frac{\Gamma(n-1/2)}{n!}\left(\frac{1}{\varepsilon}+\log\beta-\psi(2n+2k)\right). \tag{B.6}$$

If $k\leqslant 0$, this is replaced by

$$\begin{aligned}K_{\alpha,\beta}(0) = &-\frac{1}{2\sqrt{\pi}}\sum_{n=0}^{-k}\beta^{2n+2k-1}\frac{\Gamma(n-1/2)}{n!}\Gamma(1-2n-2k)\\ &-\frac{1}{2\sqrt{\pi}}\sum_{n=0}^{\infty}\frac{\beta^{2n+1}}{(2n+1)!}\frac{\Gamma(n-k+1/2)}{(n-k+1)!}\left(\frac{1}{\varepsilon}+\log\beta-\psi(2n+2)\right).\end{aligned} \tag{B.7}$$

The poles at odd integers are dealt with in like manner. We put $\alpha=2k+1+\varepsilon$ and find, for $k\geqslant 0$,

$$K_{\alpha,\beta}(0) = \frac{1}{2\sqrt{\pi}}\sum_{n=0}^{\infty}\frac{\beta^{2n+2k}}{(2n+2k)!}\frac{\Gamma(n-1/2)}{n!}\left(\frac{1}{\varepsilon}+\log\beta-\psi(2n+2k+1)\right), \tag{B.8}$$

and for $k\leqslant -1$,

$$\begin{aligned}K_{\alpha,\beta}(0) = &-\frac{1}{2\sqrt{\pi}}\sum_{n=0}^{-k-1}\beta^{2n+2k}\frac{\Gamma(n-1/2)}{n!}\Gamma(-2n-2k)\\ &+\frac{1}{2\sqrt{\pi}}\sum_{n=0}^{\infty}\frac{\beta^{2n}}{(2n)!}\frac{\Gamma(n-k-1/2)}{(n-k)!}\left(\frac{1}{\varepsilon}+\log\beta-\psi(2n+1)\right).\end{aligned} \tag{B.9}$$

We turn to the ε-expansion of series $\kappa_{1,2}$ in (B.4) and (B.5). Series κ_1 is singularity free and even finite at even integer α, so that we can use (B.4) at $\alpha=2k$. (The series terminates when the Γ-functions in the denominator become singular.) Series κ_2 is singular at even integers. We substitute $\alpha=2k+\varepsilon$ and expand, arriving at

$$\kappa_2 = \frac{1}{2\sqrt{\pi}}\sum_{n=0}^{\infty}\frac{\Gamma(n-k+1/2)}{(n-k+1)!}\frac{\beta^{2n+1}}{(2n+1)!}\left[\frac{1}{\varepsilon}+\frac{1}{2}\left(\psi(n-k+2)-\psi(k-n+\tfrac{1}{2})\right)\right] \tag{B.10}$$

for $k\leqslant 1$, and at

$$\kappa_2 = -\frac{\sqrt{\pi}}{4}\sum_{n=0}^{k-2}\frac{\Gamma(k-n-1)}{\Gamma(k-n+1/2)}\frac{\beta^{2n+1}}{(2n+1)!}+\frac{1}{2\sqrt{\pi}}\sum_{n=0}^{\infty}\frac{\Gamma(n-1/2)}{n!}\frac{\beta^{2n+2k-1}}{(2n+2k-1)!}$$
$$\times\left[\frac{1}{\varepsilon}+\frac{1}{2}\left(\psi(n+1)-\psi\left(\frac{3}{2}-n\right)\right)\right] \tag{B.11}$$

for $k \geqslant 2$.

Finally, we consider the series $\kappa_{1,2}$ at odd integer α. We put $\alpha = 2k+1+\varepsilon$ and find, for $k \leqslant 0$,

$$\kappa_1 = -\frac{1}{2\sqrt{\pi}}\sum_{n=0}^{\infty}\frac{\Gamma(n-k-1/2)}{(n-k)!}\frac{\beta^{2n}}{(2n)!}\left[\frac{1}{\varepsilon}+\frac{1}{2}\left(\psi(n-k+1)-\psi\left(k-n+\frac{3}{2}\right)\right)\right], \tag{B.12}$$

and for $k \geqslant 1$,

$$\kappa_1 = \frac{\sqrt{\pi}}{4}\sum_{n=0}^{k-1}\frac{\Gamma(k-n)}{\Gamma(k-n+3/2)}\frac{\beta^{2n}}{(2n)!}-\frac{1}{2\sqrt{\pi}}\sum_{n=0}^{\infty}\frac{\Gamma(n-1/2)}{n!}\frac{\beta^{2n+2k}}{(2n+2k)!}$$
$$\times\left[\frac{1}{\varepsilon}+\frac{1}{2}\left(\psi(n+1)-\psi\left(\frac{3}{2}-n\right)\right)\right]. \tag{B.13}$$

Series κ_2 is finite and singularity free at odd integer α, so that we can use (B.5) at $\alpha = 2k+1$.

Thus, at integer α, we can piece together series $K_{\alpha,\beta}(1)$ in (B.2) by adding the respective series in ((B.4)–(B.13)). For instance, $K_{-2,\beta}(1) = K_2(\beta)/\beta$, with the modified Bessel function K_2, which follows by putting $k=-1$ and adding $K_{\alpha,\beta}(0)$ in (B.7), κ_1 in (B.4) (with $\alpha = 2k$), and κ_2 in (B.10). There are no singularities in the first two orders of $K_{\alpha,\beta}(1)$ for $\alpha \geqslant 3$ and $\alpha \leqslant -2$, so that we can read them off from ((A.19)–(A.21)). In between, we find the leading orders at integer α as

$$K_{2,\beta}(1) = \frac{\pi}{4}+\beta\left(\log\frac{\beta}{2}+\gamma_{\mathrm{E}}\right)+\mathrm{O}(\beta^2),$$
$$K_{1,\beta}(1) = \log\frac{2}{\beta}-\gamma_{\mathrm{E}}-1+\frac{\pi}{2}\beta+\mathrm{O}(\beta^2\log\beta),$$
$$K_{0,\beta}(1) = \frac{1}{\beta}-\frac{\pi}{2}-\frac{\beta}{2}\left(\log\frac{\beta}{2}+\gamma_{\mathrm{E}}-\frac{3}{2}\right)+\mathrm{O}(\beta^3\log\beta),$$
$$K_{-1,\beta}(1) = \frac{1}{\beta^2}+\frac{1}{2}\left(\log\frac{\beta}{2}+\gamma_{\mathrm{E}}-\frac{1}{2}\right)+\mathrm{O}(\beta^2\log\beta). \tag{B.14}$$

The ε-expansion of the normalization factors $K_{\alpha,\beta}(\gamma_1)$ for $\gamma_1 > 1$ is recovered from the series representation (A.22) and (A.23). Series (A.23) is singularity free at integer α, and the ε-expansion of $K_{\alpha,\beta}(1)$ has been discussed in the foregoing. The ascending series of the hypergeometric functions in (A.23) is only efficient for γ_1 close to one. For $\gamma_1 \gg 1$, we calculate these functions via (A.24). However, in (A.24) there occur singularities at $\alpha-k = b = -(2m+1)$, $m \geqslant -1$. In this case, we calculate the hypergeometric functions in (A.23) by means of the identity

$$\frac{1}{3}(\gamma_1^2-1)^{3/2}{}_2F_1\left(\frac{3}{2},\frac{1}{2}-m;\frac{5}{2};1-\gamma_1^2\right)=\frac{\gamma_1^{2m+2}}{4\sqrt{\pi}}\sum_{\substack{n=0\\ n\neq m+1}}^{\infty}\frac{\Gamma(n-1/2)}{(n-m-1)n!}\frac{1}{\gamma_1^{2n}}$$
$$-\frac{\Gamma(m+1/2)}{4\sqrt{\pi}(m+1)!}\left(\psi(m+2)-\psi\left(\frac{1}{2}-m\right)+2\log\gamma_1\right). \quad \text{(B.15)}$$

At any other integer $b=\alpha-k$, we can use (A.24), as it is singularity free.

We finally indicate the derivation of (B.15), obtained by ε-expansion of (A.24). We start with the series (A.17); singularities occur at $b=-(2m+1)+\varepsilon$, $m\geqslant -1$. We find,

$${}_2F_1\left(-\frac{1}{2},\frac{b-1}{2};\frac{b+1}{2};\frac{1}{\gamma_1^2}\right)=\frac{1-b}{2\sqrt{\pi}}\frac{\Gamma(m+1/2)}{(m+1)!}\frac{1}{\gamma_1^{2m+2}}\frac{1}{\varepsilon}$$
$$+\frac{1-b}{4\sqrt{\pi}}\sum_{\substack{n=0\\ n\neq m+1}}^{\infty}\frac{\Gamma(n-1/2)}{(n-m-1)n!}\frac{1}{\gamma_1^{2n}}+\mathrm{O}(\varepsilon). \quad \text{(B.16)}$$

This settles the ε-expansion of the left-hand side of (A.24). On the right-hand side, we also substitute $b=-(2m+1)+\varepsilon$ and expand,

$$\frac{\sqrt{\pi}}{2}\frac{\Gamma((b+1)/2)}{\Gamma((b+2)/2)}\gamma_1^{b-1}=\frac{1-b}{2\sqrt{\pi}}\frac{\Gamma(m+1/2)}{(m+1)!}\gamma_1^{-2m-2}\frac{1}{\varepsilon}$$
$$\times\left[1+\frac{\varepsilon}{2}(\psi(m+2)-\psi(\tfrac{1}{2}-m)+2\log\gamma_1)+\mathrm{O}(\varepsilon^2)\right]. \quad \text{(B.17)}$$

Identity (B.15) follows by substituting expansions (B.16) and (B.17) into (A.24).

References

[1] A. Sommerfeld, Proc. Konink. Akad. Wet. (Sec. Sci.) 7 (1904) 346.
[2] S. Tanaka, Prog. Theor. Phys. 24 (1960) 171.
[3] Ya.P. Terletsky, Sov. Phys.-Dokl. 5 (1961) 782.
[4] G. Feinberg, Phys. Rev. 159 (1967) 1089.
[5] R. Tomaschitz, Eur. Phys. J. B 17 (2000) 523.
[6] A.S. Goldhaber, M.M. Nieto, Rev. Mod. Phys. 43 (1971) 277.
[7] R. Tomaschitz, Eur. Phys. J. D 32 (2005) 241.
[8] J.A. Wheeler, R.P. Feynman, Rev. Mod. Phys. 17 (1945) 157.
[9] R. Tomaschitz, Physica A 320 (2003) 329.
[10] R. Tomaschitz, Class. Quantum Grav. 18 (2001) 4395.
[11] G. Feinberg, Sci. Am. 222 (2) (1970) 69.
[12] D.G. Boulware, Phys. Rev. D 1 (1970) 2426.
[13] R. Newton, Science 167 (1970) 1569.
[14] F.A.E. Pirani, Phys. Rev. D 1 (1970) 3224.
[15] E. Whittaker, A History of the Theories of Aether and Electricity, Thomas Nelson & Sons, London, 1951.
[16] R. Tomaschitz, Physica A 307 (2002) 375.
[17] R. Tomaschitz, Eur. Phys. J. C 45 (2006) 493.
[18] D. Band et al., Astrophys. J. 413 (1993) 281.
[19] N.M. Lloyd, V. Petrosian, Astrophys. J. 511 (1999) 550.
[20] V. Petrosian, Astrophys. J. 557 (2001) 560.
[21] W. Magnus, F. Oberhettinger, R.P. Soni, Formulas and Theorems for the Special Functions of Mathematical Physics, Springer, New York, 1966.
[22] F. Aharonian et al., Astron. Astrophys. 432 (2005) L25.
[23] L. Sidoli et al., Astron. Astrophys. 361 (2000) 719.
[24] B.M. Gaensler, M.J. Pivovaroff, G.P. Garmire, Astrophys. J. 556 (2001) L107.

[25] H. Katagiri et al., Astrophys. J. 619 (2005) L163.
[26] F. Aharonian et al., Astron. Astrophys. 437 (2005) L7.
[27] K. Tsuchiya et al., Astrophys. J. 606 (2004) L115.
[28] F. Aharonian et al., Astron. Astrophys. 425 (2004) L13.
[29] A.F. Iyudin et al., Nature 396 (1998) 142.
[30] H. Tsunemi et al., Publ. Astron. Soc. Japan 52 (2000) 887.
[31] P. Slane et al., Astrophys. J. 548 (2001) 814.
[32] S. Mereghetti, Astrophys. J. 548 (2001) L213.
[33] O. Kargaltsev et al., Astrophys. J. 580 (2002) 1060.
[34] A.F. Iyudin et al., Astron. Astrophys. 429 (2005) 225.
[35] F. Aharonian et al., Astron. Astrophys. 439 (2005) 1013.
[36] R. Mukherjee, J.P. Halpern, Astrophys. J. 629 (2005) 1017.
[37] F. Aharonian et al., Astron. Astrophys. 435 (2005) L17.
[38] T. Sako et al., Astrophys. J. 537 (2000) 422.
[39] G.M. Dubner et al., Astron. J. 123 (2002) 337.
[40] R.N. Manchester et al., Astron. J. 129 (2005) 1993, http://www.atnf.csiro.au/research/pulsar/psrcat/.
[41] F.A. Aharonian et al., Astron. Astrophys. 460 (2006) 365.
[42] R.C. Hartman et al., Astrophys. J. Suppl. 123 (1999) 79.
[43] P.L. Nolan et al., Astrophys. J. 597 (2003) 615.
[44] B.M. Gaensler et al., Astrophys. J. 588 (2003) 441.
[45] F. Aharonian et al., Astron. Astrophys. 393 (2002) L37.
[46] F. Aharonian et al., Astron. Astrophys. 431 (2005) 197.
[47] R. Mukherjee et al., Astrophys. J. 589 (2003) 487.
[48] S. Wachter et al., Astrophys. J. 621 (2005) 393.
[49] R. Tomaschitz, Astropart. Phys. 23 (2005) 117.
[50] R. Tomaschitz, Astropart. Phys. (2007), doi:10.1016/j.astropartphys.2006.09.003.
[51] R. Tomaschitz, J. Phys. A 38 (2005) 2201.
[52] O.C. de Jager et al., Astrophys. J. 457 (1996) 253.
[53] A. Atoyan, J. Buckley, H. Krawczynski, Astrophys. J. 642 (2006) L153.
[54] C.D. Dermer, M. Bötcher, Astrophys. J. 643 (2006) 1081.
[55] R. Tomaschitz, Eur. Phys. J. C (2007), doi:10.1140/epjc/s10052-006-0168-4.
[56] M. Nagano, A.A. Watson, Rev. Mod. Phys. 72 (2000) 689.